



# Transition to a much warmer climate for the global ocean and Antarctic Ice Sheet coupled system, and its reversibility

Pierre Mathiot<sup>1</sup>, Nicolas C. Jourdain<sup>1</sup>, Benoit Urruty<sup>1</sup>, Fabien Gillet-Chaulet<sup>1</sup>, Olivier Gagliardini<sup>1</sup>, and Gael Durand<sup>1</sup>

<sup>1</sup>Univ. Grenoble Alpes/CNRS/IRD/G-INP/INRAE, Institut des Geosciences de l'Environnement, Grenoble, France.

**Correspondence:** Pierre Mathiot (pierre.mathiot@univ-grenoble-alpes.fr)

**Abstract.** In Antarctica, two plausible tipping points have been suggested: an ocean tipping point involving a cold-to-warm transition of ice shelf cavities, and an ice sheet tipping point associated with the marine ice sheet instability. This study explores the existence of such tipping points at the scale of Antarctica, using a coupled ocean–ice-sheet model. We first apply and then remove an abrupt perturbation to the ocean, instantaneously switching the atmospheric forcing to high-end 23rd century conditions, which shifts all ice shelf cavities of Antarctica to warm conditions. Our findings reveal that Antarctic continental shelf waters rapidly warm, leading to a regime shift with increased ice shelf melt rates, significant ice shelf thinning, and retreat of ice sheet grounding lines. The ocean conditions reverse over a few years when the atmospheric perturbation ceases, while the ice sheet's response is much slower. Some regions of East Antarctica show signs of ice sheet reversibility over several centuries. In contrast, we identify 14 ice streams, primarily in the Ross, Amundsen, Filchner, Ronne, and Dronning Maud Land basins, that still undergo irreversible retreat several centuries after the removal of the perturbation.

## 1 Introduction

Tipping points occur when changes in large parts of the climate system, known as tipping elements, become self-perpetuating beyond a forcing threshold (McKay et al., 2022). This involves the presence of feedbacks that amplify the response to a forcing perturbation. In this case, the system often reorganises into a state that remains stable when the perturbation is removed. As a result, plotting a state variable versus the forcing variable appears as a hysteresis with possible bistable steady states in a range of forcing values. Transitions in and out of this range can thus appear irreversible. In Antarctica, two plausible tipping points have been suggested: (i) an ocean tipping point in which an ice-shelf cavity switches from a cold state with low melt rates to a warm state with high melt rates, and (ii) an ice-sheet tipping point, often described in terms of ice-sheet instability, in which the grounded ice flow abruptly accelerates while the grounding line retreats inland.

Hellmer et al. (2017) found that the cold-to-warm ocean transition of the Filchner-Ronne cavity under future scenarios was irreversible in the sense that basal melting of the ice shelf had to be artificially suppressed to return to the original state once the atmospheric perturbation was removed. Hazel and Stewart (2020) also reported a bi-stability of the thermal state of this cavity, depending on the history of idealised wind forcing perturbations. In contrast, Haid et al. (2023) and Reese et al. (2026) gave a more contrasted picture, their reversed atmospheric perturbation experiments indicated reversibility of the Filchner-



25 Ronne cavity, although the ocean required several decades to return to its initial state. Haid et al. (2023) nonetheless identified  
some sensitivity to the initial state across a range of atmospheric forcing, which suggested some bi-stability. Additionally,  
Caillet et al. (2022) suggested that similar cold-to-warm ocean transitions may have occurred in the Amundsen Sea after  
the pre-industrial era, but reversed perturbation experiments showed reversibility within a few decades in this case. Given the  
computational cost of the ocean models used in these studies and the large number of degrees of freedom of the atmospheric  
30 forcing, the aforementioned authors were unable to conduct a large number of experiments with slow-increasing perturbations  
and multiple reversals, as done in ice sheet modelling studies (e.g., Garbe et al., 2020b; Rosier et al., 2021). This limitation  
prevented a systematic analysis of hystereses and reversibility for the ocean.

Ice sheet tipping points in Antarctica primarily involve the so-called marine ice sheet instability (MISI), which is triggered  
by ocean-induced ice shelf thinning. This instability was first mathematically identified as such by Weertman (1974) then  
35 formalized by Schoof (2007), before being simulated in numerous modelling studies (e.g., Gudmundsson et al., 2012; Favier  
et al., 2014). While the recent retreat of Antarctic grounding lines may not yet be irreversible or self-sustained (Hill et al., 2023),  
there is observational evidence of recent ocean and sea ice regime shifts (Abram et al., 2025). Further grounding line retreat  
eventually could lead to the irreversible collapse of some marine regions of West Antarctica even under present-day climate  
conditions (Reese et al., 2023). A complete collapse of the West Antarctic ice sheet may be committed if global warming  
40 reaches 2°C above pre-industrial conditions (Garbe et al., 2020a) or if the Amundsen sea warms by more than 1.2°C above  
present-day conditions (Rosier et al., 2021) or even less (Chandler et al., 2025). However, confidence in the parameterised  
ice-shelf melt rates under future conditions remains low (Burgard et al., 2022, 2023).

This study investigates the reversibility of the ocean cold-to-warm transition in 25 major ice shelf cavities of Antarctica, as  
well as the potential for cascading effects, specifically, whether ocean–ice-sheet feedbacks promote irreversibility. To address  
45 these questions, we use a coupled ocean–ice-sheet model at relatively high resolution, here 0.25°. As described in Mathiot and  
Jourdain (2023) (hereafter MJ2023) strong perturbations of the atmosphere are required to trigger a cold-to-warm transition  
across all Antarctic ice shelves. In this study, we therefore focus on the reversibility of the ocean–ice-sheet response to the  
large scale perturbation used in MJ2023.

## 2 Ocean–sea-ice–ice-shelf simulations

### 50 2.1 Coupled ocean/sea-ice/ice-sheet Model

The ocean–ice-sheet model used in this study consists of a coupling between the NEMO global ocean component and the  
Elmer/Ice Antarctic ice sheet component. These two components were previously coupled in a very simple configuration  
representing a single ice shelf (Favier et al., 2019), but the coupling framework has been completely revised since then. The  
two individual components and the coupling interface are described hereafter. Some experiments make use of the standalone  
55 Elmer/Ice model (i.e., uncoupled to NEMO), with the same model set-up, except for ice shelf basal melting, which is prescribed  
in the standalone version.



### 2.1.1 Ocean/sea-ice component: NEMO

We use version 4.0.4 of the three-dimensional primitive-equation ocean–sea-ice model NEMO (Nucleus for European Modelling of the Ocean; Madec et al., 2019). The model is configured on a global grid with a nominal horizontal resolution of 0.25° (approximately 8 km at 70°S), which is sufficient to represent the main features of ocean circulation beneath Antarctic ice shelves (Mathiot et al., 2017). A comprehensive description and evaluation of this configuration are provided in MJ2023; here, only the key elements are outlined. The vertical discretisation relies on a  $z^*$  coordinate system (Adcroft and Campin, 2004), using 121 levels with variable spacing: resolution is about 1 m near the surface, around 20 m between 100 m and 1000 m depth, and becomes coarser in deeper layers. Sea-ice processes are simulated with the SI3 model (Rousset et al., 2015), while icebergs are represented as Lagrangian particles (Marsh et al., 2015; Merino et al., 2016). Basal melting beneath ice shelves is computed using the three-equation formulation (Holland and Jenkins, 1999; Asay-Davis et al., 2016). In this framework, the effect of tides is included via a spatially varying background velocity derived from the CATS2008 model (Padman et al., 2008), following the approach of Jourdain et al. (2019). The bathymetry of the Antarctic continental shelf, as well as the ice shelf draft, are prescribed from BedMachine Antarctica version 2 (Morlighem et al., 2020; Morlighem, 2020).

### 2.1.2 Ice sheet component: Elmer/Ice

We use the Elmer/Ice model to simulate the evolution of the ice sheet (Gagliardini et al., 2013). The configuration employed here is briefly described below, while a comprehensive presentation is available in Hill et al. (2023). Ice flow is computed by solving the Shallow Shelf Approximation (SSA) to the Stokes equations, assuming an isotropic rheology described by Glen’s flow law. The initial ice sheet geometry is prescribed from BedMachine Antarctica version 2 (Morlighem et al., 2020; Morlighem, 2020). Ice viscosity and basal friction are inferred by inversion using ice thickness observations primarily from 2009–2019 (Morlighem et al., 2020; Morlighem, 2020) together with surface ice velocity data from a 2015–2016 snapshot provided by the MEaSUREs Annual Ice Velocity Maps dataset (Mouginot et al., 2019). The viscosity and friction parameters are kept constant in time. In floating regions, where inversion is not applicable, basal friction is set to a constant value of  $1 \text{ Pa m}^{-1} \text{ a}$ , consistent with a linear Weertman sliding law (Weertman, 1974).

Boundary conditions assume fixed ice shelf front positions, and no basal melting is applied beneath grounded ice or partially floating grid cells. The surface mass balance is derived from the climatology of the atmosphere–snow model of van Wessem et al. (2018) and is held constant throughout the simulations, as the focus is on ocean–ice-sheet tipping processes. The representation of basal mass balance is described in Section 2.1.3. The grounding line position is determined using a flotation criterion, and basal friction in partially floating elements is treated using a sub-grid parameterisation (SEP3; Seroussi et al., 2014). The computational mesh is anisotropic, with a horizontal resolution ranging from 1 km near the grounding line to 50 km in the interior, and remains fixed during the simulations.

Prior to the prognostic simulations, a relaxation phase is performed to limit inconsistencies between the initial input fields and the inverted state when transitioning from diagnostic to prognostic simulation (Gillet-Chaulet et al., 2012). The model is first integrated for 5 years using the linear Weertman sliding law (Weertman, 1974), consistent with the inversion procedure



90 used to derive basal friction coefficients. This initial phase is followed by an additional 15 years of relaxation employing  
a regularised Coulomb friction law (Joughin et al., 2019). The corresponding parameters are obtained from the previously  
inverted linear friction coefficients, following Brondex et al. (2019).

### 2.1.3 The ocean–ice-sheet coupling interface

In the coupled configuration, exchanges between NEMO and Elmer/Ice are performed annually. Ocean-induced basal melt  
95 rates computed by NEMO are provided to Elmer/Ice, while Elmer/Ice supplies NEMO with iceberg calving fluxes and updated  
ice-shelf basal topography. The two models are run sequentially over each coupling interval: NEMO first simulates ocean  
dynamics over one year and provides the corresponding annual mean basal mass balance beneath ice shelves, after which  
Elmer/Ice simulates ice sheet evolution over the same period and returns the updated ice-shelf geometry along with yearly  
averaged calving rates. Within this framework, no temporal lag is introduced for basal melt rates between the two models.  
100 In contrast, the ice-shelf topography used by NEMO progressively lags behind that simulated by Elmer/Ice, ranging from no  
delay at the beginning of the year to approximately one year at its end. Additionally, calving fluxes used in NEMO’s Lagrangian  
iceberg model are delayed by one year relative to the ice dynamics simulated by Elmer/Ice. This coupling strategy is broadly  
consistent with previous approaches described by Smith et al. (2021) and Pelletier et al. (2022).

The interpolation of Elmer/Ice topography to each NEMO grid point is made using the natural finite element interpolation  
105 from Elmer/Ice. Calving rates are transposed onto the NEMO grid by routing, for each coastal Elmer/Ice element, the calving  
flux toward the nearest NEMO ocean cell. The interpolation of the NEMO melt rate onto the Elmer grid is first obtained  
through a conservative interpolation. Then, because of inconsistencies between the grounding lines of NEMO and Elmer/Ice,  
any ice shelf mesh of Elmer/Ice with no corresponding ice shelf mesh in NEMO is filled with melt rates from the nearest ice  
shelf cells. Conversely, if the conservative interpolation gives a non-zero melt rate beneath a grounded mesh in Elmer/Ice, it is  
110 set to zero.

In the absence of an evolving calving front and for the sake of numerical stability of the ice-sheet model, we keep imposing a  
minimum ice shelf thickness of 1 m in the coupled system. Beneath such 1 m ice, basal melt rates are still simulated in NEMO,  
and the 1 m capping imposed in Elmer/Ice is equivalent to a spurious mass flux injected in the coupled system, i.e. there is  
no mass conservation. The importance of melting in these areas, hereafter referred to as “pseudo-collapsed areas” is presented  
115 with our results.

## 2.2 Experiments

To build the initial state of the coupled model, we start from a first guess consisting of the ice sheet geometry after the 20-year  
relaxation described in section 2.1.2 and the ocean state from the year 1999 of MJ2023’s reference (after 20 years of spin-  
up). This produces inconsistent initial conditions between Elmer/Ice and NEMO because the ocean state and geometry of the  
120 under-ice shelf cavities provided by the Elmer/Ice initialisation differ from those in the standalone versions. To reduce this  
inconsistency, that can be locally large, the first-guess ocean state is extrapolated to fit the Elmer/Ice topography at the end of  
the relaxation, and NEMO is run for 5 more years with this steady topography. Then Elmer/Ice is run for an additional 5 years

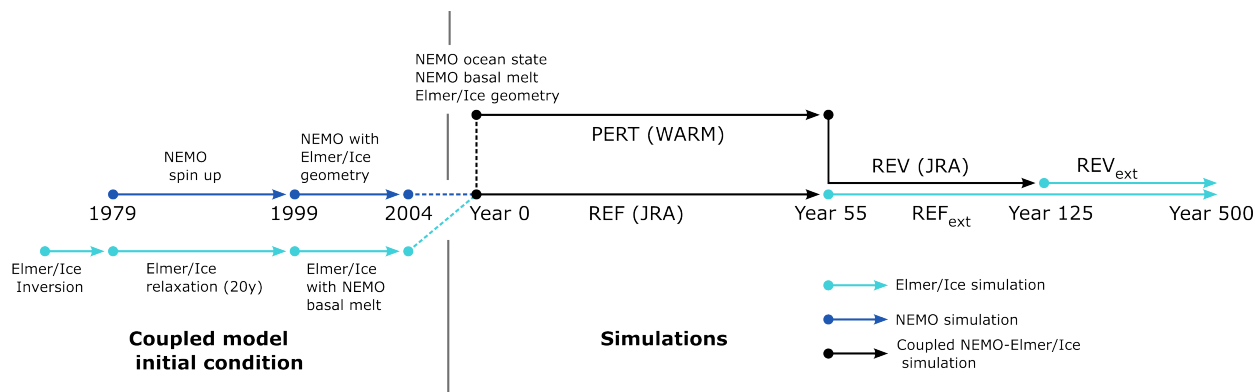


**Figure 1.** Illustration of the coupled model initialization procedure (left) and the simulation protocol (right).

beyond the first guess, with the basal melt computed by NEMO in its 5<sup>th</sup> year. A schematic of the initialisation procedure is available in Fig. 1.

125 The additional 5-year ocean relaxation is sufficient to flush most of the cavities and bring basal melt rates into equilibrium with the updated ice geometry. The subsequent 5-year ice sheet relaxation allows the ice sheet to adjust rapidly to the changes in basal melt, while slower adjustments occur over the first decades of the simulation. Since this study primarily compares results with a reference simulation, these longer-term, slow adjustments do not affect our conclusions.

This initialized state is subsequently used for three main experiments: the reference simulation (REF), a perturbed scenario (PERT), and a reversibility run (REV), as described below and in Table 1.

In terms of atmospheric forcing, our strategy is almost identical to that of MJ2023. The reference experiment (REF) is a present-day simulation driven by the JRA55-do version 1.4 atmospheric reanalysis (Tsuji et al., 2018), which provides 3-hourly atmospheric fields at 55 km resolution and captures realistic interannual variability over the period 1858-2018. In this study, we restrict the JRA period to the satellite era (1979-2018). The perturbed experiment (PERT) is an idealised abrupt shift to high-end atmospheric conditions representative of the end of the 23rd century. PERT starts from the same initial state as 135 REF. We also run a reversibility experiment (REV), which begins from the last year of PERT and is subsequently driven by the same atmospheric forcing as REF.

The atmospheric forcing applied in PERT follows MJ2023. It retains both the mean state and interannual variability of JRA55-do, onto which monthly anomalies are superimposed for all variables used in the computation of ocean surface bound- 140 ary conditions. These anomalies are defined as the difference between 2260–2299 and 1975–2014 and are derived from monthly outputs of the IPSL-CM6A-LR climate model (Boucher et al., 2020) under the SSP5-8.5 emission scenario (Meinshausen et al., 2020). In all experiments, the ice-sheet surface mass balance is prescribed from the climatology of van Wessem et al. (2018) and is held constant in time, so that the simulated ice-sheet evolution reflects only ocean–ice-sheet interactions.

Given the high computational cost of coupled simulations, we run PERT and REF for 55 years and REV for 70 years. 145 To extend the simulation beyond the 1979–2018 period, we repeat the 40-year forcing period in a continuous loop. Within



**Table 1.** List of coupled and standalone ice sheet simulations with their main characteristics. (REF+REF<sub>ext</sub>) covers 500 years, and so does (REF+REV+REV<sub>ext</sub>).

Experience name	Type	Length	Atm. forcing of the ocean	Initial conditions
REF	Coupled	55 a	JRA	see Sec. 2.1.3
PERT	Coupled	55 a	JRA+perturbation	same as REF
REV	Coupled	70 a	JRA	PERT (last year)
REV <sub>ext</sub>	standalone ice sheet	375 a	N/A	REV (last year)
REF <sub>ext</sub>	standalone ice sheet	445 a	N/A	REF (last year)

each cycle, the forcing is identical. This approach, commonly used in ocean modelling (Griffies et al., 2016), introduces discontinuities in the atmospheric forcing at the transition between cycles. To investigate the slow component of ice sheet reversibility, which can exceed 70 years, we extend REV through standalone ice sheet simulations, which are computationally less demanding than coupled simulations. These extended simulations (hereafter REV<sub>ext</sub>) start from the final ice sheet state of REV and are forced with a constant ice shelf basal mass balance derived from the last year of REV. REV<sub>ext</sub> spans 375 years after the end of REV. To account for potential ice sheet model drift, we also extend REF using Elmer/Ice, hereafter REF<sub>ext</sub>, for an additional 445 years. From this point onward, all years are defined relative to the initial condition of REF, with year 0 corresponding to the first year of the simulation.

A summary of all the simulations presented here is available in Table 1 and visualized in Fig 1.

### 155 3 Ocean tipping points

#### 3.1 Results

The ocean responses to the strong atmospheric perturbation are very similar in the ocean–ice-shelf coupled simulations and in the standalone experiments analysed in MJ2023: sea ice is no longer formed, leading to a collapse of dense water formation. Consequently, the density barrier between the cold dense shelf water and the warm Circumpolar Deep Water (CDW) offshore disappears, and the CDW penetrates onto the continental shelves in the Ross, Weddell, Amery, and East Antarctica sectors. This leads to an ocean warming at depth of +4 to +5°C at these locations (Fig. 2a). The CDW water mass also becomes warmer, so that the present-day warm shelves already under the influence of CDW (Amundsen and Bellingshausen seas) warm by +1 to +2°C (Fig.2a).

The continental shelf becomes a warm-fresh type all around Antarctica, as defined in MJ2023, with a westward surface current above the shelf break and an eastward or near-zero current near the sea floor, favouring the intrusion of CDW (Fig. 3). These changes in shelf properties lead to a tenfold increase in average basal melt rates beneath the Antarctic ice shelves, from 1,204 (REF) to 15,783 (PERT) Gt a<sup>-1</sup>, consistent with MJ2023.

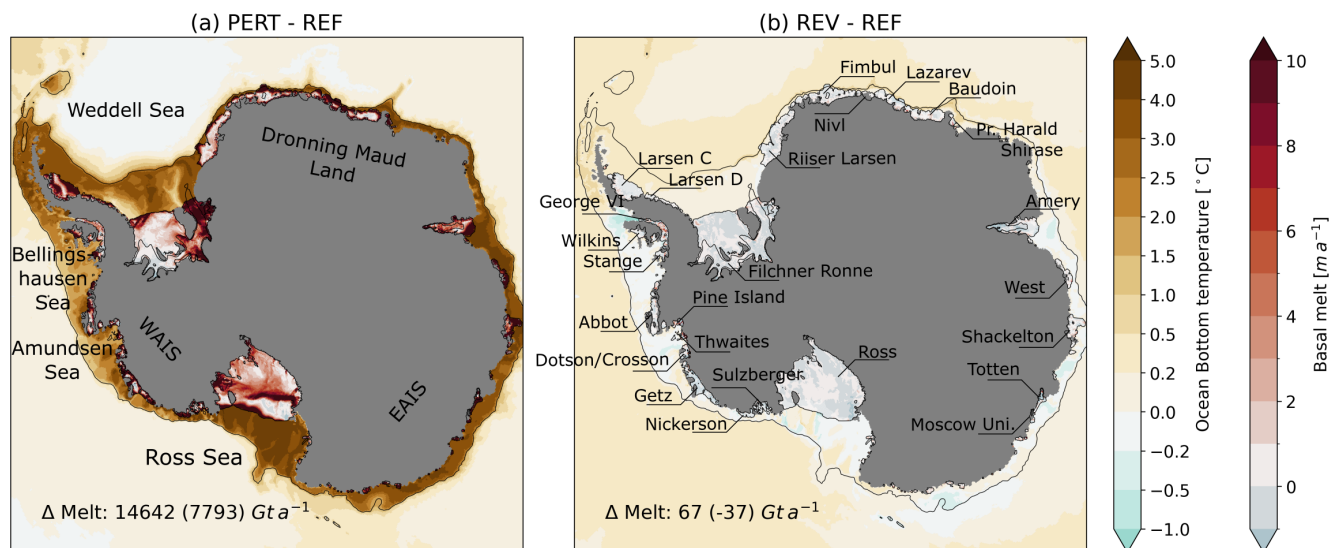


**Figure 2.** Ocean bottom temperature (blue to brown colour bar) and basal melt rate (blue to red colour bar) anomaly (a) due to the atmospheric perturbation (PERT minus REF, averaged from their 46<sup>th</sup> to 55<sup>th</sup> years), and (b) after removal of the atmospheric perturbation (REV averaged from its 61<sup>st</sup> to 70<sup>th</sup> year minus REF averaged from its 46<sup>th</sup> to 55<sup>th</sup> year). The differences in total basal melt between the two simulations are indicated in the lower left corners. Numbers in brackets are the melt differences estimated only beneath the non vanished ice shelf cells ( $h_{ice} > h_{min}$ ).

There are nonetheless some differences in ice shelf basal melt rates between our coupled simulations and the standalone ocean simulations of MJ2023. For the reference simulation, these differences are mainly observed at Getz and George VI. In 170 MJ2023, due to the absence of feedback between basal melt rates and ice shelf draft depth in the presence of a strong ocean thermocline bias, the melt rate was much higher than observed for George VI. The melt rate bias for the Getz ice shelf in MJ2023 was such that the draft was artificially thinned to mitigate the impact of the ocean bias in front of the ice shelf. In this study, the feedback between the ocean and the ice sheet allows Elmer/Ice to rapidly adjust to a shallower ice draft, deviating from the initial inverse topography. As a result, parts of the ice shelf draft stabilize in colder water, leading to more realistic 175 melt rates with respect to Rignot et al. (2013) estimates.

For the perturbed experiment, the first difference with MJ2023 is that weaker melt rates are simulated beneath the inner part of ice shelves (because they thin in the coupled experiments, sometimes moving above the thermocline). This is compensated by stronger melt rates at the grounding line and a generally larger ice shelf area due to grounding line retreat (not shown). It is worth noting that 49% of the melt in the perturbed experiment occurs in the pseudo-collapsed areas where the ice shelf reaches 180 the minimum thickness of 1 m allowed by Elmer/Ice (Fig. 2). The fraction of melt occurring in these pseudo-collapsed areas varies greatly from one ice shelf to another, e.g., 8% for Filchner-Ronne and 91% for Larsen D (Fig. 4). The impact of non-stop melting in the pseudo-collapsed areas is discussed in Sec. 5.

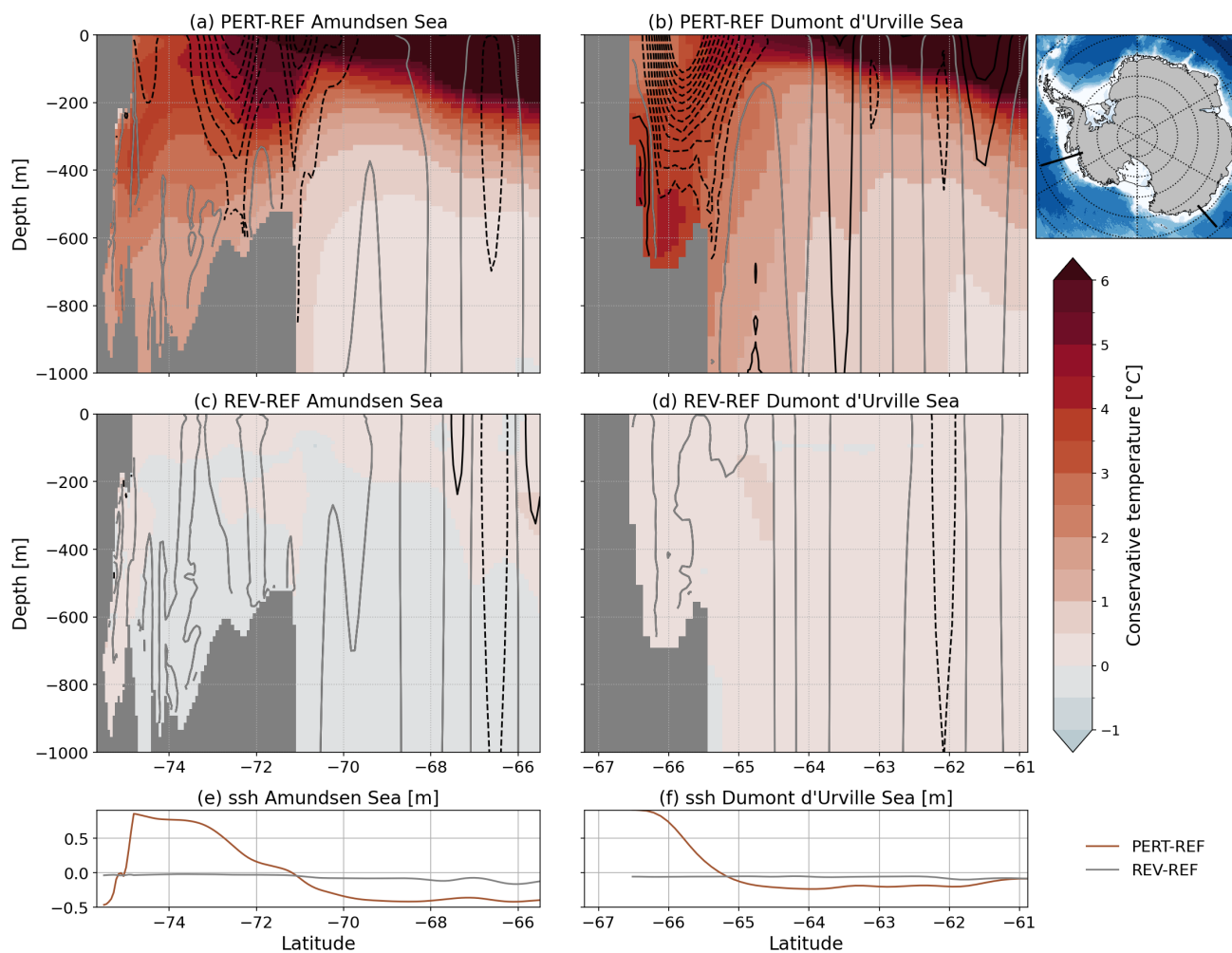


**Figure 3.** (a–c) Temperature differences along a vertical section across the Amundsen Sea: (a) Differences between PERT and REF and (b) between REV and REF. (b–d) Temperature differences along a cross-section across the Dumont d’Urville Sea: (b) Differences between PERT and REF and (d) Between REV and REF. The same years as in Fig. 2 are used to calculate these differences. The black contours show the zonal velocity differences every  $5 \text{ cm s}^{-1}$  (dashed/solid lines for westward/eastward velocity differences), gray line for zero velocity difference. (e–f) Sea surface height difference profile along the corresponding sections between PERT and REF (brown) and REV and REF (gray).

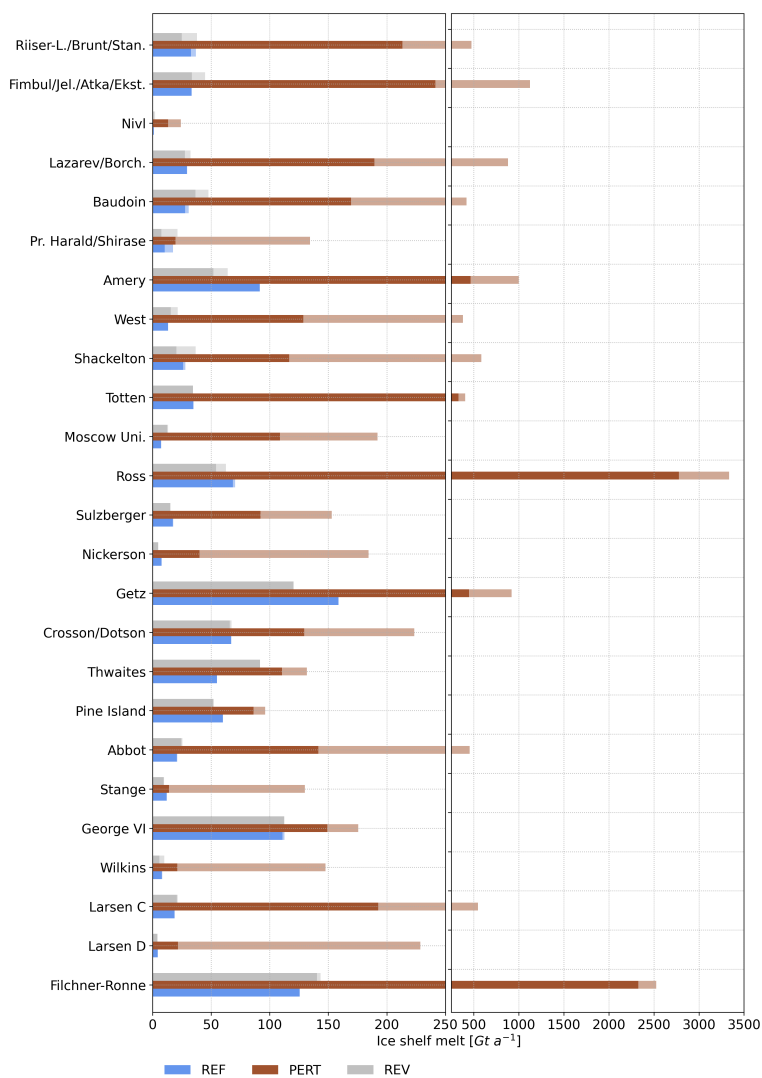


**Figure 4.** Total basal melt per ice shelf (in  $Gt a^{-1}$ ) in PERT (blue) and REF (brown). For clarity, only ice shelves (or groups of ice shelves) larger the  $4000 km^2$  are represented ( $\sim 70\%$  of the total ice shelf area, Rignot et al., 2013). The lighter parts of the bars indicate the contribution of the pseudo-collapsed area ( $h_{ice} \leq 1m$ ). Location of each ice shelves is shown in Fig. 2b



Ocean properties on the continental shelf appear to be entirely reversible within 70 years. Switching back to the reference atmospheric forcing is enough to restart sea ice formation and brine rejection. This triggers the formation of new HSSW that spreads on all former dense shelves, rebuilding shelf dense water and the density barrier that prevents intrusion of warm CDW (Fig. 3). The brine rejection also regenerates the cold winter surface mixed layer and the Antarctic Surface Water (AASW). These features are key to the formation of fresh shelves (Thompson et al., 2018). Furthermore, the CDW cools back to the reference value. This allows the Amundsen and Bellingshausen Seas to return to their present day properties (Fig. 3). Consequently, the end state of the reversibility experiment is very similar to the reference state (Fig. 2b). The reversal of ocean properties on various shelves begins immediately after the atmospheric forcing is reversed, as does the ice shelf basal melt, and takes approximately 40 years to complete (Fig. 5ab). The reversibility of iceberg melt is closely linked to the timescale required for iceberg calving to recover from the perturbation. Since calving is proportional to ice shelf thickness and velocity, its reversibility follows the timescale of the ice sheet rather than that of the ocean. Consequently, returning to the REF iceberg melt state takes more than 70 years (Fig. 5c), but the deficit remains limited and does not seem to affect the ocean reversibility.

The integrated melt per ice shelf is reversible for most of the ice shelves (Fig. 4) and for Antarctica (integrated difference of  $67 \text{ Gt a}^{-1}$ , i.e.,  $\sim 5\%$ , between REV and REF). This is a balance between the thinner ice shelves at the end of the coupled REV experiment, which tend to reduce the thermal forcing, and a larger ice shelf area because the grounding line do not return to their original positions after 70 years (Fig. 6b). The abrupt increase in melting is not fully reversible beneath three ice shelves, Thwaites, Getz and Amery, for which noticeable differences are found between REV and REF (Fig. 4). Getz and Amery melt less after the reversibility experiment than in the reference. This is due to thinner ice shelves inducing a lower thermal driving both due to the pressure dependence of the freezing point and to the displacement of the ice draft toward the cold surface layer. These changes outweigh the effects of the increase in ice shelf area. In contrast, Thwaites melts more after the reversibility experiment because the grounding line retreat exposes a large ice area to CDW (Fig. 7).

### 3.2 Discussion on the ocean transition and its reversibility

As in MJ2023, our results indicate that transitions from cold to warm cavities do occur for all Antarctic ice shelves under conditions between the present-day climate and a plausible realisation of 2300 under SSP5-8.5. Our method is not appropriate for the identification of atmospheric thresholds that lead to abrupt warming in ice shelf cavities under gradually changing atmospheric conditions. The relatively high resolution required to simulate a large number of ice shelves makes it computationally difficult to produce large ensemble of simulations, which would be required to address tipping points in a more systematic way, as done in Garbe et al. (2020a) for the Antarctic ice sheet.

A new result is that transitions to a warm state appear to be reversible within 40 years for most shelves in our simulations (Fig. 5). It is important to stress that this was estimated by assuming that the atmospheric state can be reversed instantaneously, which is not realistic. We nonetheless believe that these results are useful for understanding the climate system, as they indicate that the Southern Ocean itself would not contribute making large climate transitions irreversible.

The reversibility of the Filchner-Ronne cold-to-warm transition reported in this study is consistent with Reese et al. (2026) and somewhat consistent with Haid et al. (2023), but differs from Hellmer et al. (2017) and Hazel and Stewart (2020), who

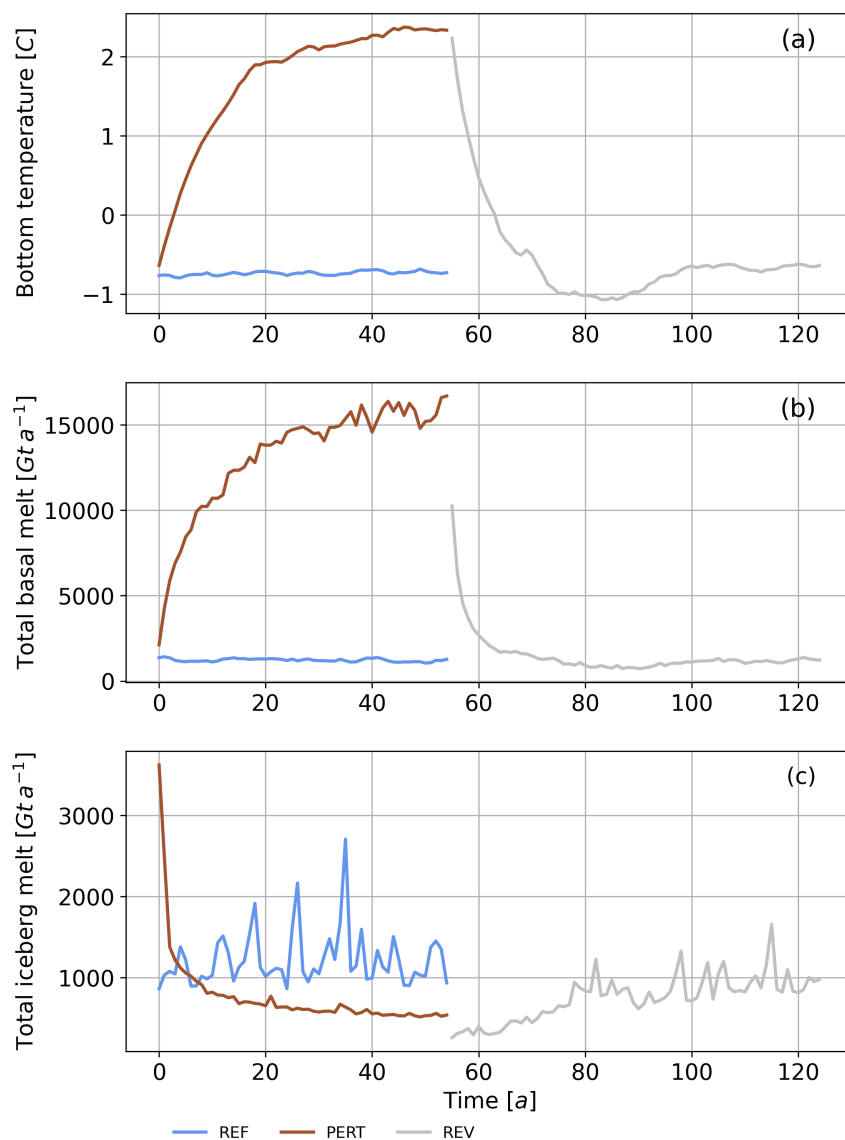


**Figure 5.** (a) Time series of bottom temperature average over Antarctica continental shelf (bathymetry shallower than 1000 m), (b) integrated ice shelf basal melt, and (c) integrated iceberg melt.

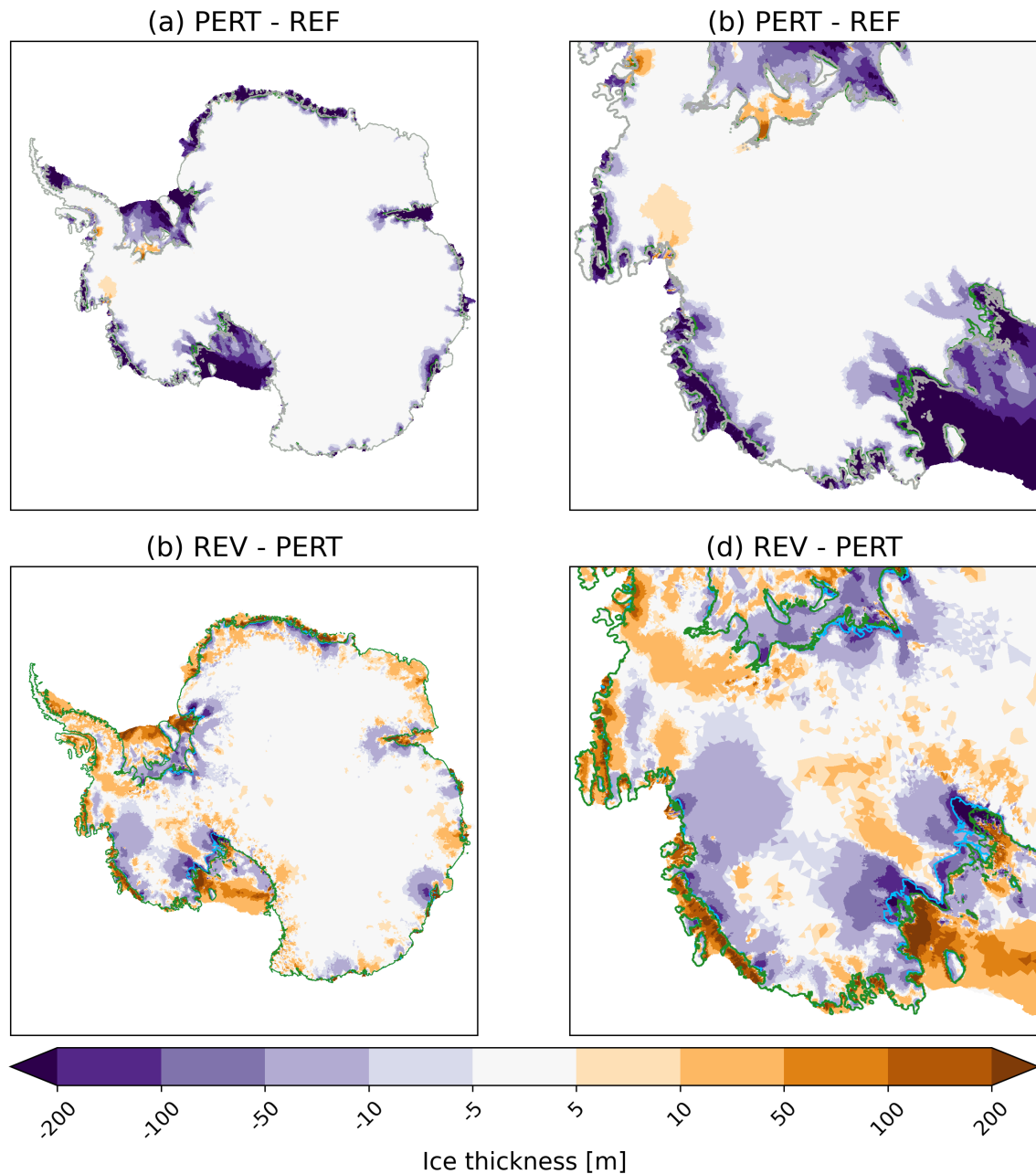


**Figure 6.** Ice thickness anomaly (a) after 55 years of atmospheric perturbation (PERT at year 55, i.e. at the end of the coupled PERT simulation) w.r.t. REF(year 55, i.e. at the end of the coupled REF simulation), and (c) after 70 more years of reversed atmospheric forcing (REV at year 70, i.e. at the end of the coupled REV simulation) w.r.t. (PERT at year 55, i.e. at the end of the coupled PERT simulation). (b) and (d) are respectively zoomed-in views of (a) and (c). In grey, green and blue the grounding line position in REF, PERT and REV, respectively.



identified a hysteresis behaviour (see introduction). The perturbation methods differ across these studies, so it is difficult to find an explanation for these differences. First, our findings do not rule out the existence of a hysteresis in the melt response to the atmospheric forcing, but if there is a hysteresis, it must be narrower than the perturbation that we impose. In this case, it would mean that our transitions jump from one side of the hysteresis to the other, hence appearing as reversible. Second, the position of the tipping/reversal threshold is determined by the interplay between the activity of the Ronne ice-shelf polynya (Moorman et al., 2023; Saddier et al., 2026), basal melting beneath Filchner-Ronne (Hellmer et al., 2017), and advection from the westward coastal current (Hazel and Stewart, 2020; Bull et al., 2021). Therefore, any model bias or difference in the modelling setup may impact the tipping behaviour. In particular, the polynya activity may be strongly impacted by the resolution and fidelity of the atmospheric forcing (e.g., reanalyses in our study and Haid et al., 2023, vs coarse climate model in Hellmer et al., 2017), and by the use of constant ocean lateral boundary conditions (Hellmer et al., 2017; Hazel and Stewart, 2020) vs global ocean simulations (this study and Haid et al., 2023).

Very few studies have so far investigated ocean tipping points and their reversibility outside of Filchner-Ronne. Caillet et al. (2022) showed that surface buoyancy fluxes were the main drivers of multi-decadal transitions between cold and warm states in the Amundsen Sea. They did not identify any hysteresis in these long-term regime shifts, although their interannual transitions between cold periods and warmer periods can be interpreted as an indication of bi-stability (Moorman et al., 2023).

For the Ross Ice Shelf, a possible reversibility for large transitions is supported by paleo-proxies suggesting a warm-to-cold transition during the mid-Holocene (Lowry et al., 2024). The main suggested driver of such a transition is an increase in polynya activity, which leads to a strengthening of the HSSW formation, flooding the Ross shelf with cold water. This mechanism is similar to the one simulated in our reversibility experiment. However, reversibility may only apply to very large atmospheric shifts, such as the one applied in this study, and may not occur for smaller perturbations. Hysteresis effects, where the ocean remains in a warm state despite the cessation of perturbation, could emerge under more moderate perturbations, as demonstrated by Garbe et al. (2020a) for the Antarctic Ice Sheet.

## 4 Ice sheet tipping points

### 4.1 Results

We then assess the response of individual ice drainage basins to the changes in oceanic conditions during the coupled perturbation (PERT) and reversibility (REV) experiments, as well as during the standalone ice-sheet extension ( $REV_{ext}$ ). For this purpose, three variables are analysed: the flux at the grounding line (GL), the integrated grounding area, which is used as a proxy for the GL position, and the volume above flotation (VAF), which indicates the ice sheet contribution to changes in sea level.

The strong increase in melt rates induced by the ocean in response to the atmospheric perturbations leads to a pronounced thinning of all ice shelves, exceeding 200 m in many places after 55 years (Fig. 6a). The extent of thinning is so severe that some ice shelves, such as Getz, Abbot, and Larsen, entirely reach a pseudo-collapsed state (yellow area in Fig. 7). At most locations, such ice shelf thinning leads to a strong loss of buttressing (Fürst et al., 2016), which accelerates the upstream ice

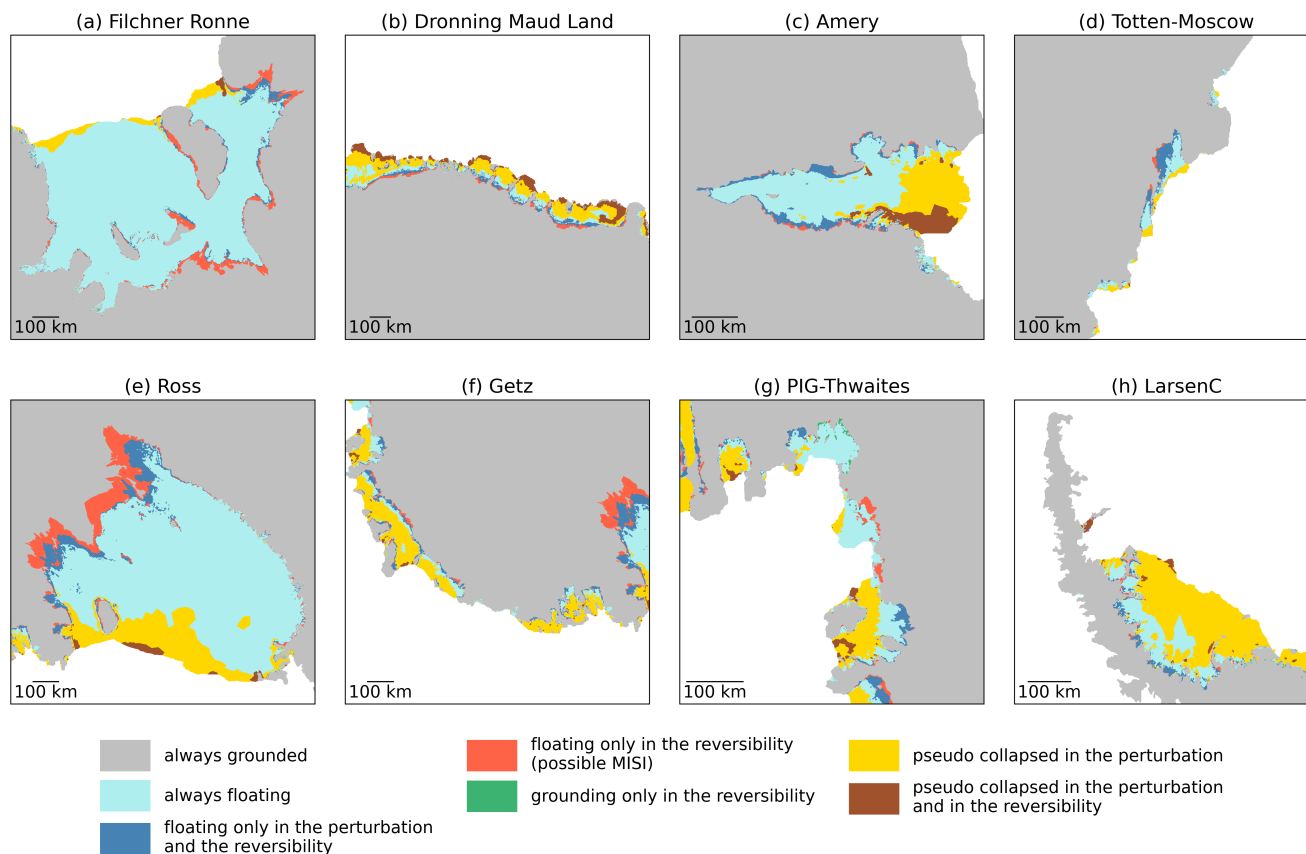


**Figure 7.** Area types (grounded, floating, and collapsed) at the end of REF, PERT, and REV. Gray (turquoise) represents areas that are always grounded (floating). Yellow (brown) indicates areas that are collapsed at the end of PERT (and remain collapsed at the end of REV). Blue (red) shows areas that become ungrounded during PERT (and stay ungrounded in REV). Green represents areas that are grounded only in REV.

250 streams (not shown), resulting in a rapid increase in ice transport across the grounding line. The total ice flux across the GL in Antarctica nearly doubles in PERT compared to REF (Fig. 8a). This thinning also causes the retreat of GLs across all major basins, particularly for the Filchner-Ronne, Ross, Thwaites, and Dronning Maud Land ice shelves (Fig. 7).

The reversibility of the ice sheet is much more complex than that of the ocean due to the varying characteristics of the basins and the slower response time of the ice sheet to increased melt rates, which goes beyond the PERT and REV period and motivated the extension through standalone simulations. After 500 years of simulation (encompassing the PERT, REV, and REV<sub>ext</sub> phases), the sector of East Antarctica including the Enderby, Amery, Princess Elisabeth, Aurora Subglacial, and Wilkes Subglacial basins shows signs of reversibility: ice flux at the GL rapidly returns to its reference value (Fig. 8a), the GL slowly re-advances toward its position in the reference simulation (Fig. 8b), and mass above flotation is gradually re-approaching

255



the reference simulation (Fig. 8c). Other ice drainage basins, like Filchner-Ronne, Dronning Maud Land (Baudouin, Fimbul  
260 and Coats), Ross and Amundsen are showing signs of instability: their mass above flotation keeps diverging after 500 years  
(Fig. 8c).

However, by looking at individual streams, the picture is very contrasted. The instabilities of Filchner-Ronne, Dronning  
Maud Land, Ross, and Amundsen ice basins are driven by only a few streams (Fig. 9). Thwaites, Ice Stream A to E feeding  
the Ross Ice Shelf, Baudouin, Borchgrevink, Fimbul, and Riiser-Larsen feeding the Dronning Maud Land Ice Shelves and the  
265 Bailey, Slessor, and Institute ice streams feeding the Filchner-Ronne Ice Shelf continue to retreat despite the removal of the  
perturbation (see Fig. 9 for the locations). These streams also lose mass at a faster rate than in the reference simulation (Fig. 9),  
indicating a degree of instability with possible MISI (Schoof, 2007).

Nevertheless, when examining various indicators such as flux at the GL, GL position, and VAF, it becomes evident that  
reversibility is dependent on both the timescale and the metrics used. With the exception of Thwaites, all the aforementioned  
270 ice streams show reversible fluxes at the GL over a timescale shorter than the 500 years studied here (Fig. 10a), despite their  
continued mass loss relative to the  $REF_{ext}$  (Fig. 10c). For most of these ice streams, the GL continues to retreat inland for  
the first 200 years after the reversibility experiment began. However, a few of them continue to retreat inland until the end of  
the 500-year simulation (Ice Stream A and B in the Ross Basin, Thwaites Glacier, Institute ice streams in the Filchner-Ronne  
Basin, and Fimbul, Borchgrevink, and Baudouin ice streams in Dronning Maud Land). This indicates that these streams might  
275 have entered a MISI. The others eventually stabilize or readvance.

The reversibility of the ice shelves is also slower than the 70-year duration of the REV phase. Notably, certain areas remain  
in a "pseudo-collapsed" state even after the reversibility phase (brown areas in Fig. 7). These regions, where the ice thickness is  
reduced to 1 meter, are particularly prone to regrowth, more so than if a complete collapse had occurred, as they may experience  
positive snow accumulation and frazil ice formation. The fact that these areas do not exhibit significant regrowth suggests that  
280 their growth by ice advection is too slow to counterbalance the basal melt. Furthermore, even for areas that always remain  
afloat (turquoise areas in Fig. 7), the recovery of ice shelf thickness is slower than the REV timescale. Fig. 6 shows that many  
ice shelves lose more than 200 meters of ice and recover only between 5 and 100 meters at the front.

## 4.2 Discussion

Our experimental framework, while not designed to identify specific thresholds for ocean warming that trigger regime shifts  
285 in ice sheet dynamics, demonstrates that a short (55-year) but intense atmospheric perturbation over the ocean can induce  
instability in certain Antarctic ice basins. Notably, these instabilities persist as irreversible retreat over the 500-year timescale  
of our study and likely beyond for specific ice catchment basins and ice streams, despite the ocean returning to present-day  
conditions within 40 years. This underscores the asymmetry in reversibility between ocean and ice sheet responses, a critical  
insight for understanding long-term climate commitments.

290 At the basin scale, the integrated trends in GL positions reveal that most basins either re-advance immediately or after a  
delay following the perturbation. However, some basins, such as the Wilkes Subglacial Basin, are known for their potential  
instability. While Mengel and Levermann (2014) and Garbe et al. (2020a) demonstrate that extensive GL retreat in the Wilkes

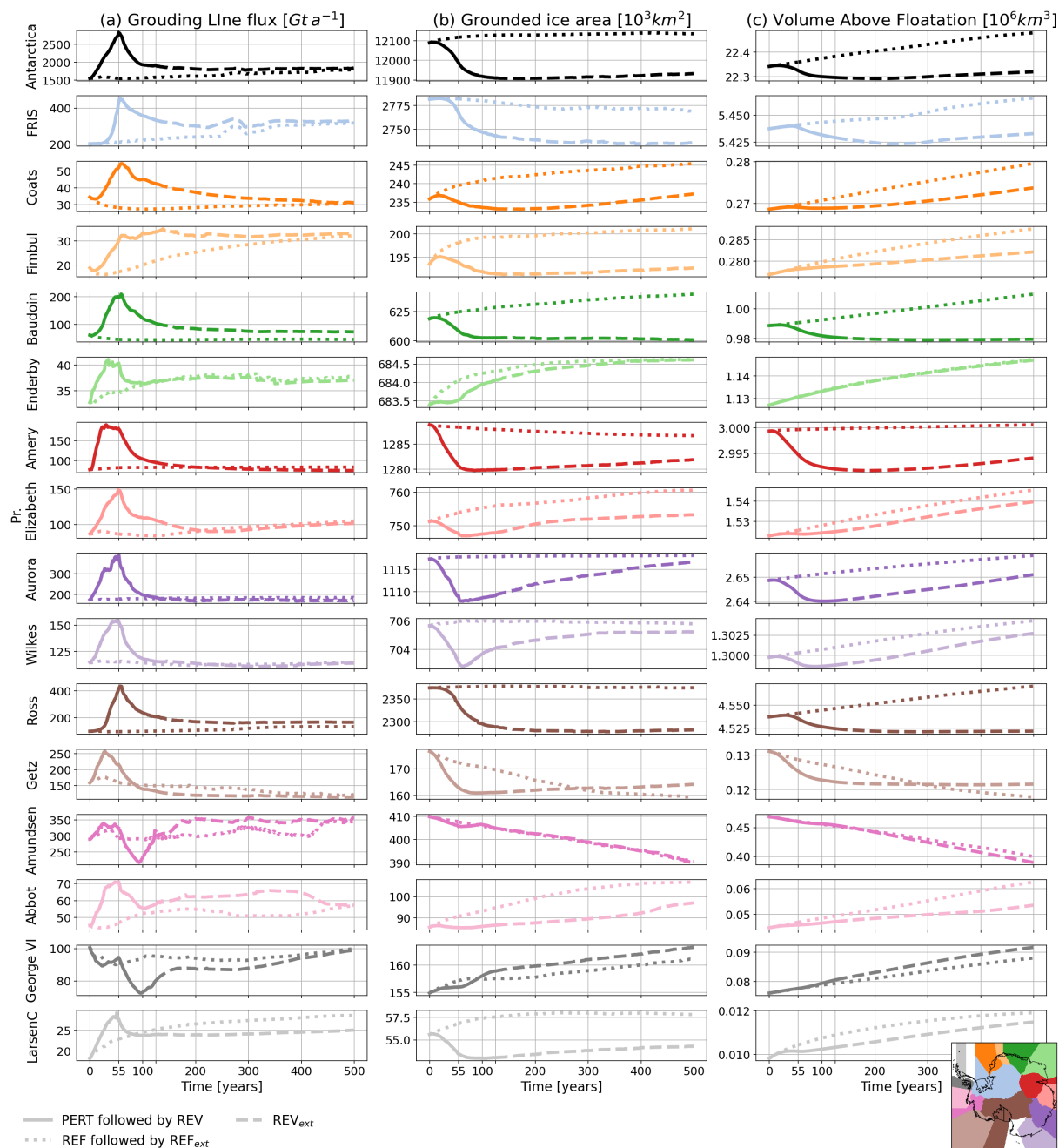


**Figure 8.** Time series of (a) grounding line flux, (b) grounded ice area, (c) volume above flotation for the whole Antarctica (black, upper panels) and individual ice drainage basins (see corresponding colours on the map in the lower right corner). Results are displayed for PERT and REV (solid line),  $REV_{ext}$  (dashed) and REF and its extension (dotted). Only the basins with grounding line flux of more than  $15 \text{ Gt a}^{-1}$  at the start of the simulations are represented.

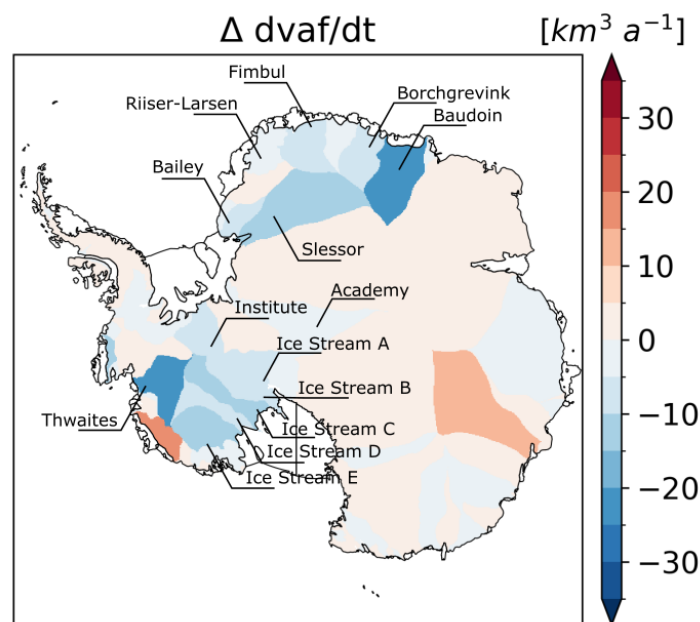


**Figure 9.** Difference between variation rate of volume above floatation (vaf) between REV and REF at the end of the simulation (year 500).

Subglacial Basin can trigger irreversible collapse, our simulations show only a modest ice loss ( $\sim 1,200$  Gt), far below the  $\sim 30,000$  Gt required to remove the protective "ice plug". This discrepancy likely arises from the short duration of our perturbation, which may not have been sufficient to reach the tipping point. Similarly, the Aurora Subglacial Basin, another region prone to irreversible retreat (Garbe et al., 2020a), shows no signs of instability in our simulations, further suggesting that longer or stronger perturbations are necessary to cross critical thresholds.

Our study highlights that basin-scale analyses alone are insufficient to assess ice sheet stability. Within individual basins, specific ice streams, such as Baudouin, Borchgrevink, Institute, Jutulstraumen, Thwaites, Mercer, and Whillans, continue to retreat even after 350 years of reversibility. This indicates that stability assessments must account for the behaviour of individual ice streams, as their responses can diverge significantly from basin-wide trends.

The reversibility of GL positions occurs over longer timescales compared to GL flux, consistent with findings from standalone ice sheet models (Hill et al., 2023). Our simulations also align with grounding line retreat patterns observed in the UKESM Earth System Model (Siahaan et al., 2022) and other standalone models (Seroussi et al., 2024; Reese et al., 2023). However, a notable exception is the behaviour of Pine Island Glacier (PIG).

Favier et al. (2014) demonstrated that PIG is on the edge of an irreversible retreat. Other studies also support the fact that PIG may be unstable under various forcing (Seroussi et al., 2024; Reese et al., 2023). However, in our simulations, PIG shows no signs of retreat—neither during the perturbation nor during the reversibility phase. Instead, the grounding line advances onto the latest subglacial ridge. This behaviour in Elmer/Ice is consistent with Hill et al. (2023) and is a long standing issue.

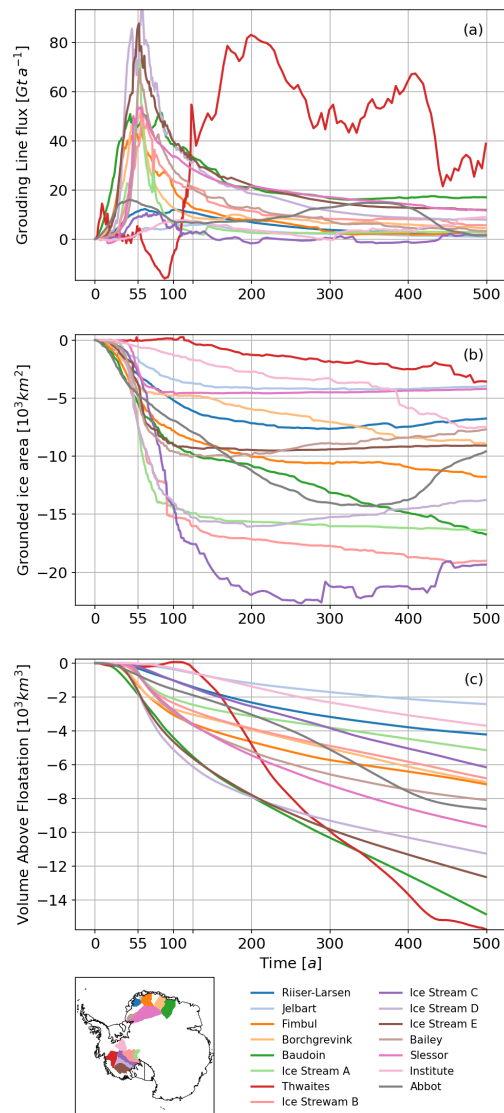


**Figure 10.** (a) Anomaly of grounding line flux in PERT then REV with respect to REF. (b) As (a) but for the grounded ice area (proxy for grounding line advance or retreat). (c) As (a) but for the volume above floatation.



310 One likely reason is the insufficient melt rates at the GL, as discussed in MJ2023, which prevents the grounding line from retreating.

In contrast to PIG, the nearby Thwaites Glacier exhibits irreversible inland retreat. Gudmundsson et al. (2023) demonstrated that Thwaites's behaviour was complex, with limited sensitivity to ice shelf collapse at century timescales, with minimal SLR contribution due to weak buttressing from its current ice shelf configuration. In addition, their work highlighted a strong  
315 sensitivity to the friction law, ice sheet model, and model setup, as well as spatial heterogeneity in the response. Thwaites East gains mass after ice shelf removal, while Thwaites West loses mass, reflecting contrasting regional dynamics.

In our simulations, Thwaites initially responds with limited grounding line retreat and VAF changes over the first 100 years, consistent with Gudmundsson et al. (2023). However, beyond this period, the grounding line retreats inland, triggering rapid ice flux acceleration and VAF decline. This nonlinear transition suggests that Thwaites may remain stable under short-term  
320 perturbations but could undergo accelerated retreat once critical thresholds are surpassed, aligning with Joughin et al. (2014). While the exact conditions for triggering such instability are beyond our scope, our results underscore the potential for delayed but significant destabilization in response to ocean forcing perturbations.

Direct comparisons between the various studies remain challenging due to differences in experimental setups, including forcing scenarios, model configurations, and timescales. Nonetheless, our findings contribute to the growing evidence that ice  
325 sheet responses to climate perturbations are highly nonlinear, with critical implications for future projections.

## 5 General discussion

Although our model provides an advanced representation of ocean–ice shelf interactions, the high computational cost imposes several limitations. Three key aspects are particularly affected: (i) the spin-up procedure with standalone components does not achieve a perfect balance between the different components of the coupled model, (ii) the use of fixed melt rates in the  
330 extended simulation period may limit the model's ability to capture long-term feedbacks between ice shelf geometry and melt rates, especially in regions of strong thermocline (as in Getz ice shelf, for example), and (iii) the computational constraints prevent a systematic exploration of tipping points through multiple small perturbation experiments and reversibility analyses.

There are also caveats related to structural limitations of our models. In particular, ice damage and calving may increase the irreversibility of ice acceleration and thinning. Here, ice damage and calving front position are assumed to be constant. Our  
335 approach in the coupling framework has been to keep a minimum ice shelf thickness of 1 m, while still calculating melt rates in the ocean model. The overestimated meltwater flux may amplify the ocean warming at depth (Bett et al., 2020; Caillet et al., 2022), but does not prevent reversibility. A real front retreat of ice-shelf collapse would also change the ocean heat transport into the ice shelf cavity (Bradley et al., 2022), with a lot of uncertainty related to the presence of sea ice and polynyas in the deglaciated areas. Maintaining these 1-m ice shelf areas also facilitates the regrowth under cold conditions, compared to a real  
340 ice shelf front that would need to readvance little by little.



## 6 conclusions

In this study, we introduced a new coupled ocean–ice–sheet model, inspired by the idealized work of Favier et al. (2019). This work represents a preliminary step toward the future integration of the Elmer/Ice ice sheet model into an Earth System Model.

To investigate whether regime shifts in Antarctic shelf waters can trigger glaciological tipping points in the Antarctic ice sheet, we used an approach similar to that of MJ2023, but within a coupled ocean–ice–sheet framework. To achieve this, we applied a strong and abrupt perturbation to atmospheric conditions, typical of the year 2300 under the SSP5-8.5 scenario (MJ2023), over the ocean for 55 years. Following this perturbation, we conducted an abrupt reversibility experiment, returning to present-day conditions for 70 years.

Consistent with the forced simulation results of MJ2023, our perturbed simulations reveal that the entire Antarctic continental shelf experiences substantial warming within the first two decades of perturbation, with several additional decades required for the largest ice shelf cavities to adjust. In the absence of HSSW production, the intrusion of CDW onto the formerly cold continental shelves of the Ross, Weddell, and East Antarctica regions becomes more pronounced. These changes in oceanic properties lead to a significant increase in ice shelf melt rates, with total basal mass loss escalating from 1,200 to 15,800 Gt a<sup>-1</sup> after 55 years of perturbation.

The reversibility experiment demonstrated that all Antarctic shelf waters are capable of reversing to their original state within a relatively short period. The primary mechanism identified is the resumption of convection due to brine formation with the return to present-day conditions. This leads to the formation of HSSW, spreading across the shelves and preventing CDW intrusion. Furthermore, the brine rejection facilitates the rebuilding of the surface cold mixed layer, and AASW and the northward migration of winds upon returning to present-day conditions contributes to restoring the typical fresh shelves.

As expected, the substantial increase in basal melt rates in the perturbation leads to the thinning of ice shelves, acceleration of ice streams, and retreat of ice sheet grounding lines in most sectors. Additionally, several ice shelves (including the Larsen, Abbot, Cosgrove, Dotson/Crosson, Getz, and others) have experienced pseudo-collapse. When atmospheric conditions are reverted to present-day levels, grounding line flux begins to decrease, and grounding line positions start advancing toward their reference state in many ice drainage basins and streams. However, this reversibility process is much slower for the ice sheet than for the ocean, taking over 100 years for grounding line flux and more than 500 years for grounding line positions to stabilize. We have identified 14 ice streams, primarily in the Ross, Amundsen, Filchner, Ronne, and Dronning Maud Land basins, that appear to undergo irreversible retreat (indicated by a growing difference in VAF between the reference and reversibility experiments over time). These findings align with Reese et al. (2023), though the reversibility of these streams depends significantly on the metrics and timescales considered.

Overall, all Antarctic ice shelf cavities can switch to warm conditions at some level of global warming, triggering a strong response in ice sheet dynamics. This study confirms the irreversible nature of the Antarctic ice sheet mass loss, pointing out that this behaviour is related to a small number of ice streams. In our modelling framework, we have not identified circumstances in which an irreversible change in the ice landscape would cause the ocean to tip to a different stable state.



375 *Code availability.* The Elmer/Ice code is available here: <https://github.com/ElmerCSC/elmerfem> at Version: 9.0 (commit: 21ddff3a). The extra ELmer/ice solvers, the NEMO source code, and the parameter namelists for each experiment are all available in Mathiot et al. (2026).

*Data availability.* Data used to run the simulations are available upon request to the lead author. Scripts used to generate the figures, and the simulation outputs required to produce the plots are all available in Mathiot et al. (2026).

*Author contributions.* All authors contributed to the experimental design and to the discussion of ideas and results. BU performed the Elmer/Ice inversion. PM set up and ran all simulations. PM led the writing of the manuscript, with contributions from all authors.

380 *Competing interests.* N. C. Jourdain is an editor of The Cryosphere. The authors declare no other competing interest.

*Acknowledgements.* This study was funded by the European Union's Horizon 2020 research and innovation programme under grant agreements No 820575 (TiPACCs) and No 101003536 (ESM2025), by the French National Research Agency under Grant ANR-19-CE01-0015 (EIS) and from the support of the French Government through the France 2030 program managed by ANR (ISCLim, ANR-22-EXTR-0010).  
385 This work was granted access to the HPC resources of CINES and TGCC under allocations A0120106035 and A0140106035 attributed by GENCI. We acknowledge the use of AI tools to improve the writing style of the manuscript.



## References

- Abram, N. J., Purich, A., England, M. H., McCormack, F. S., Strugnell, J. M., Bergstrom, D. M., Vance, T. R., Stål, T., Wienecke, B., Heil, P., et al.: Emerging evidence of abrupt changes in the Antarctic environment, *Nature*, 644, 621–633, 2025.
- 390 Adcroft, A. and Campin, J. M.: Rescaled height coordinates for accurate representation of free-surface flows in ocean circulation models, *Ocean Modell.*, 7, 269–284, <https://doi.org/10.1016/j.ocemod.2003.09.003>, 2004.
- Asay-Davis, X. S., Cornford, S. L., Durand, G., Galton-Fenzi, B. K., Gladstone, R. M., Gudmundsson, G. H., Hattermann, T., Holland, D. M., Holland, D., Holland, P. R., et al.: Experimental design for three interrelated Marine Ice-Sheet and Ocean Model Intercomparison Projects, *Geosci. Model Dev.*, 9, 2471–2497, 2016.
- 395 Bett, D. T., Holland, P. R., Naveira Garabato, A. C., Jenkins, A., Dutrieux, P., Kimura, S., and Fleming, A.: The impact of the Amundsen Sea freshwater balance on ocean melting of the West Antarctic Ice Sheet, *J. Geophys. Res. Oceans*, 125, e2020JC016305, 2020.
- Boucher, O., Servonnat, J., Albright, A. L., Aumont, O., Balkanski, Y., Bastrikov, V., Bekki, S., Bonnet, R., Bony, S., Bopp, L., et al.: Presentation and evaluation of the IPSL-CM6A-LR climate model, *J. Adv. Model. Ea. Sys.*, 12, e2019MS002010, 2020.
- Bradley, A. T., Bett, D. T., Dutrieux, P., De Rydt, J., and Holland, P. R.: The Influence of Pine Island Ice Shelf Calving on Basal Melting, *J. Geophys. Res. Oceans*, 127, e2022JC018621, <https://doi.org/https://doi.org/10.1029/2022JC018621>, e2022JC018621 2022JC018621, 2022.
- 400 Brondex, J., Gillet-Chaulet, F., and Gagliardini, O.: Sensitivity of centennial mass loss projections of the Amundsen basin to the friction law, *Cryosphere*, 13, 177–195, 2019.
- Bull, C. Y. S., Jenkins, A., Jourdain, N. C., Vaňková, I., Holland, P. R., Mathiot, P., Hausmann, U., and Sallée, J.-B.: Remote control of 405 Filchner-Ronne ice shelf melt rates by the Antarctic slope current, *J. Geophys. Res. Oceans*, 126, e2020JC016550, 2021.
- Burgard, C., Jourdain, N. C., Reese, R., Jenkins, A., and Mathiot, P.: An assessment of basal melt parameterisations for Antarctic ice shelves, *Cryosphere*, 16, 4931–4975, <https://doi.org/10.5194/tc-16-4931-2022>, 2022.
- Burgard, C., Jourdain, N. C., Mathiot, P., Smith, R. S., Schäfer, R., Caillet, J., Finn, T. S., and Johnson, J. E.: Emulating present and future simulations of melt rates at the base of Antarctic ice shelves with neural networks, *J. Adv. Model. Ea. Sys.*, 15, e2023MS003829, 2023.
- 410 Caillet, J., Jourdain, N. C., and Mathiot, P.: Abrupt cold-to-warm and warm-to-cold ocean transitions in the Amundsen Sea, *Antarctica, J. Geophys. Res. Oceans*, 0, 0–0, 2022.
- Chandler, D. M., Langebroek, P. M., Reese, R., Albrecht, T., Garbe, J., and Winkelmann, R.: Antarctic Ice Sheet tipping in the last 800,000 years warns of future ice loss, *Commun. Ea. Env.*, 6, 420, 2025.
- Favier, L., Durand, G., Cornford, S. L., Gudmundsson, G. H., Gagliardini, O., Gillet-Chaulet, F., Zwinger, T., Payne, A. J., and Le Brocq, 415 A. M.: Retreat of Pine Island Glacier controlled by marine ice-sheet instability, *Nat. Clim. Change*, 4, 117–121, 2014.
- Favier, L., Jourdain, N. C., Jenkins, A., Merino, N., Durand, G., Gagliardini, O., Gillet-Chaulet, F., and Mathiot, P.: Assessment of Sub-Shelf Melting Parameterisations Using the Ocean-Ice Sheet Coupled Model NEMO (v3. 6)-Elmer/Ice (v8. 3), *Geosci. Model Dev.*, 2019.
- Fürst, J. J., Durand, G., Gillet-Chaulet, F., Tavard, L., Rankl, M., Braun, M., and Gagliardini, O.: The safety band of Antarctic ice shelves, *Nat. Clim. Change*, 6, 479–482, <https://doi.org/10.1038/nclimate2912>, 2016.
- 420 Gagliardini, O., Zwinger, T., Gillet-Chaulet, F., Durand, G., Favier, L., de Fleurian, B., Greve, R., Malinen, M., Martín, C., Råback, P., Ruokolainen, J., Sacchetti, M., Schäfer, M., Seddik, H., and Thies, J.: Capabilities and performance of Elmer/Ice, a new-generation ice sheet model, *Geosci. Model Dev.*, 6, 1299–1318, <https://doi.org/10.5194/gmd-6-1299-2013>, 2013.



- Garbe, J., Albrecht, T., Levermann, A., Donges, J. F., and Winkelmann, R.: The hysteresis of the Antarctic Ice Sheet, *Nature*, 585, 538–544, <https://doi.org/10.1038/s41586-020-2727-5>, 2020a.
- 425 Garbe, J., Albrecht, T., Levermann, A., Donges, J. F., and Winkelmann, R.: The hysteresis of the Antarctic Ice Sheet, *Nature*, 585, 538–544, <https://doi.org/10.1038/s41586-020-2727-5>, 2020b.
- Gillet-Chaulet, F., Gagliardini, O., Seddik, H., Nodet, M., Durand, G., Ritz, C., Zwinger, T., Greve, R., and Vaughan, D. G.: Greenland ice sheet contribution to sea-level rise from a new-generation ice-sheet model, *Cryosphere*, 6, 1561–1576, 2012.
- Griffies, S. M., Danabasoglu, G., Durack, P. J., Adcroft, A. J., Balaji, V., Böning, C. W., Chassignet, E. P., Curchitser, E., Deshayes, J.,  
430 Drange, H., et al.: OMIP contribution to CMIP6: Experimental and diagnostic protocol for the physical component of the Ocean Model Intercomparison Project, *Geosci. Model Dev.*, 9, 3231–3296, 2016.
- Gudmundsson, G. H., Krug, J., Durand, G., Favier, L., and Gagliardini, O.: The stability of grounding lines on retrograde slopes, *Cryosphere*, 6, 1497–1505, 2012.
- Gudmundsson, G. H., Barnes, J. M., Goldberg, D. N., and Morlighem, M.: Limited Impact of Thwaites Ice Shelf on Future Ice Loss  
435 From Antarctica, *Geophys. Res. Lett.*, 50, e2023GL102880, <https://doi.org/https://doi.org/10.1029/2023GL102880>, e2023GL102880 2023GL102880, 2023.
- Haid, V., Timmermann, R., Gürses, O., and Hellmer, H. H.: On the drivers of regime shifts in the Antarctic marginal seas, exemplified by the Weddell Sea, *Ocean Science*, 19, 1529–1544, <https://doi.org/10.5194/os-19-1529-2023>, 2023.
- Hazel, J. E. and Stewart, A. L.: Bistability of the Filchner-Ronne Ice Shelf Cavity Circulation and Basal Melt, *J. Geophys. Res. Oceans*, 125,  
440 e2019JC015848, <https://doi.org/https://doi.org/10.1029/2019JC015848>, e2019JC015848 10.1029/2019JC015848, 2020.
- Hellmer, H. H., Kauker, F., Timmermann, R., and Hattermann, T.: The fate of the southern Weddell Sea continental shelf in a warming climate, *J. Climate*, 30, 4337–4350, 2017.
- Hill, E. A., Urruty, B., Reese, R., Garbe, J., Gagliardini, O., Durand, G., Gillet-Chaulet, F., Gudmundsson, G. H., Winkelmann, R., Chekki, M., Chandler, D., and Langebroek, P. M.: The stability of present-day Antarctic grounding lines – Part 1: No indication of marine ice sheet  
445 instability in the current geometry, *Cryosphere*, 17, 3739–3759, <https://doi.org/10.5194/tc-17-3739-2023>, 2023.
- Holland, D. M. and Jenkins, A.: Modeling thermodynamic ice-ocean interactions at the base of an ice shelf, *J. Phys. Oceanogr.*, 29, 1787–1800, 1999.
- Joughin, I., Smith, B. E., and Medley, B.: Marine ice sheet collapse potentially under way for the Thwaites Glacier Basin, West Antarctica, *Science*, 344, 735–738, 2014.
- 450 Joughin, I., Smith, B. E., and Schoof, C. G.: Regularized Coulomb Friction Laws for Ice Sheet Sliding: Application to Pine Island Glacier, Antarctica, *Geophysical Research Letters*, 46, 4764–4771, <https://doi.org/10.1029/2019GL082526>, 2019.
- Jourdain, N. C., Molines, J.-M., Le Sommer, J., Mathiot, P., Chanut, J., de Lavergne, C., and Madec, G.: Simulating or prescribing the influence of tides on the Amundsen Sea ice shelves, *Ocean Modell.*, 133, 44–55, 2019.
- Lowry, D. P., Han, H. K., Gollledge, N. R., Gomez, N., Johnson, K. M., and McKay, R. M.: Ocean cavity regime shift reversed West Antarctic  
455 grounding line retreat in the late Holocene, *Nat. Commun.*, 15, 3176, <https://doi.org/10.1038/s41467-024-47369-3>, 2024.
- Madec, G., Bourdallé-Badie, R., Chanut, J., Clementi, E., Coward, A., Ethé, C., Iovino, D., et al.: NEMO ocean engine (v4.0), *Scientific Notes of Climate Modelling Center (27)* – ISSN 1288-1619, Tech. rep., <https://doi.org/10.5281/zenodo.3878122>, 2019.
- Marsh, R., Ivchenko, V. O., Skliris, N., Alderson, S., Bigg, G. R., Madec, G., Blaker, A. T., Aksenov, Y., Sinha, B., Coward, A. C., et al.:  
460 NEMO-ICB (v1. 0): interactive icebergs in the NEMO ocean model globally configured at eddy-permitting resolution, *Geosci. Model Dev.*, 8, 1547–1562, 2015.



- Mathiot, P. and Jourdain, N. C.: Southern Ocean warming and Antarctic ice shelf melting in conditions plausible by late 23rd century in a high-end scenario, *Ocean Science*, 19, 1595–1615, <https://doi.org/10.5194/os-19-1595-2023>, 2023.
- Mathiot, P., Jenkins, A., Harris, C., and Madec, G.: Explicit and parametrised representation of under ice shelf seas in az\* coordinate ocean model NEMO 3.6, *Geosci. Model Dev.*, 10, 2849–2874, 2017.
- 465 Mathiot, P., Jourdain, N., Urruty, B., Gillet-Chaulet, F., Gagliardini, O., and Durand, G.: Transition to a much warmer climate for the global ocean and Antarctic Ice Sheet coupled system, and its reversibility, <https://doi.org/10.5281/zenodo.18682049>, 2026.
- McKay, D. I. A., Staal, A., Abrams, J. F., Winkelmann, R., Sakschewski, B., Loriani, S., Fetzer, I., Cornell, S. E., Rockström, J., and Lenton, T. M.: Exceeding 1.5°C global warming could trigger multiple climate tipping points, *Science*, 377, eabn7950, <https://doi.org/10.1126/science.abn7950>, 2022.
- 470 Meinshausen, M., Nicholls, Z. R. J., Lewis, J., Gidden, M. J., Vogel, E., Freund, M., Beyerle, U., Gessner, C., Nauels, A., Bauer, N., et al.: The shared socio-economic pathway (SSP) greenhouse gas concentrations and their extensions to 2500, *Geosci. Model Dev.*, 13, 3571–3605, 2020.
- Mengel, M. and Levermann, A.: Ice plug prevents irreversible discharge from East Antarctica, *Nat. Clim. Change*, 4, 451–455, <https://doi.org/10.1038/nclimate2226>, 2014.
- 475 Merino, N., Le Sommer, J., Durand, G., Jourdain, N. C., Madec, G., Mathiot, P., and Tournadre, J.: Antarctic icebergs melt over the Southern Ocean : climatology and impact on sea-ice, *Ocean Modell.*, 104, 99–110, 2016.
- Moorman, R., Thompson, A. F., and Wilson, E. A.: Coastal polynyas enable transitions between high and low West Antarctic ice shelf melt rates, *Geophys. Res. Lett.*, 50, e2023GL104724, 2023.
- Morlighem, M.: MEASUREs BedMachine Antarctica, Version 2, Tech. rep., Boulder, Colorado USA. NASA National Snow and Ice Data Center Distributed Active Archive Center, <https://doi.org/10.5067/E1QL9HFQ7A8M>, 2020.
- 480 Morlighem, M., Rignot, E., Binder, T., Blankenship, D., Drews, R., Eagles, G., Eisen, O., Ferraccioli, F., Forsberg, R., Fretwell, P., et al.: Deep glacial troughs and stabilizing ridges unveiled beneath the margins of the Antarctic ice sheet, *Nature Geosci.*, 13, 132–137, 2020.
- Mouginot, J., Rignot, E., and Scheuchl, B.: Continent-Wide, Interferometric SAR Phase, Mapping of Antarctic Ice Velocity, *Geophysical Research Letters*, 46, 9710–9718, <https://doi.org/https://doi.org/10.1029/2019GL083826>, 2019.
- 485 Padman, L., Erofeeva, S. Y., and Fricker, H. A.: Improving Antarctic tide models by assimilation of ICESat laser altimetry over ice shelves, *Geophys. Res. Lett.*, 35, 2008.
- Pelletier, C., Fichefet, T., Goosse, H., Haubner, K., Helsen, S., Huot, P.-V., Kittel, C., Klein, F., van Lipzig, N. P. M., Marchi, S., et al.: PARASO, a circum-Antarctic fully coupled ice-sheet–ocean–sea-ice–atmosphere–land model involving f.ETISH1.7, NEMO3.6, LIM3.6, COSMO5.0 and CLM4.5, *Geosci. Model Dev.*, 15, 553–594, 2022.
- 490 Reese, R., Garbe, J., Hill, E. A., Urruty, B., Naughten, K. A., Gagliardini, O., Durand, G., Gillet-Chaulet, F., Gudmundsson, G. H., Chandler, D., Langebroek, P. M., and Winkelmann, R.: The stability of present-day Antarctic grounding lines – Part 2: Onset of irreversible retreat of Amundsen Sea glaciers under current climate on centennial timescales cannot be excluded, *Cryosphere*, 17, 3761–3783, <https://doi.org/10.5194/tc-17-3761-2023>, 2023.
- Reese, R., De Rydt, J., and Naughten, K.: Regime shift of the Filchner-Ronne Ice Shelf cavity under extreme global warming remains reversible, *J. Geophys. Res. Oceans*, submitted, 0, 0–1, 2026.
- 495 Rignot, E., Jacobs, S., Mouginot, J., and Scheuchl, B.: Ice-shelf melting around Antarctica, *Science*, 341, 266–270, 2013.
- Rosier, S. H. R., Reese, R., Donges, J. F., De Rydt, J., Gudmundsson, G. H., and Winkelmann, R.: The tipping points and early warning indicators for Pine Island Glacier, West Antarctica, *Cryosphere*, 15, 1501–1516, <https://doi.org/10.5194/tc-15-1501-2021>, 2021.



- Rousset, C., Vancoppenolle, M., Madec, G., Fichet, T., Flavoni, S., Barthélemy, A., Benschila, R., Chanut, J., Lévy, C., Masson, S., et al.:  
500 The Louvain-La-Neuve sea ice model LIM3.6: global and regional capabilities, *Geosci. Model Dev.*, 8, 2991–3005, 2015.
- Saddier, L., Herbert, C., Bull, C. Y. S., and Coustou, L.-A.: Irreversible Transitions of the Ocean Circulation in Antarctic Ice-Shelf Cavities,  
Submitted to *Geophys. Res. Lett.*, 2026.
- Schoof, C.: Ice sheet grounding line dynamics: Steady states, stability, and hysteresis, *J. Geophys. Res.*, 112, 2007.
- Seroussi, H., Morlighem, M., Rignot, E., Mouginot, J., Larour, E., Schodlok, M., and Khazendar, A.: Sensitivity of the dynamics of Pine  
505 Island Glacier, West Antarctica, to climate forcing for the next 50 years, *Cryosphere*, 8, 1699–1710, 2014.
- Seroussi, H., Pelle, T., Lipscomb, W. H., Abe-Ouchi, A., Albrecht, T., Alvarez-Solas, J., Asay-Davis, X., Barre, J.-B., Berends, C. J., Bernales,  
J., Blasco, J., Caillet, J., Chandler, D. M., Coulon, V., Cullather, R., Dumas, C., Galton-Fenzi, B. K., Garbe, J., Gillet-Chaulet, F., Glad-  
stone, R., Goelzer, H., Gollledge, N., Greve, R., Gudmundsson, G. H., Han, H. K., Hillebrand, T. R., Hoffman, M. J., Huybrechts, P.,  
Jourdain, N. C., Klose, A. K., Langebroek, P. M., Leguy, G. R., Lowry, D. P., Mathiot, P., Montoya, M., Morlighem, M., Nowicki, S.,  
510 Pattyn, F., Payne, A. J., Quiquet, A., Reese, R., Robinson, A., Saraste, L., Simon, E. G., Sun, S., Twarog, J. P., Trusel, L. D., Urruty, B.,  
Van Breedam, J., van de Wal, R. S. W., Wang, Y., Zhao, C., and Zwinger, T.: Evolution of the Antarctic Ice Sheet Over the Next Three  
Centuries From an ISMIP6 Model Ensemble, *Earth's Future*, 12, e2024EF004561, <https://doi.org/https://doi.org/10.1029/2024EF004561>,  
e2024EF004561 2024EF004561, 2024.
- Siahaan, A., Smith, R. S., Holland, P. R., Jenkins, A., Gregory, J. M., Lee, V., Mathiot, P., Payne, A. J., Ridley, J. K., and Jones, C. G.: The  
515 Antarctic contribution to 21st-century sea-level rise predicted by the UK Earth System Model with an interactive ice sheet, *Cryosphere*,  
16, 4053–4086, <https://doi.org/10.5194/tc-16-4053-2022>, 2022.
- Smith, R. S., Mathiot, P., Siahaan, A., Lee, V., Cornford, S. L., Gregory, J. M., Payne, A. J., Jenkins, A., Holland, P. R., Ridley, J. K.,  
et al.: Coupling the UK Earth System Model to dynamic models of the Greenland and Antarctic ice sheets, *J. Adv. Model. Ea. Sys.*, 13,  
e2021MS002520, 2021.
- 520 Thompson, A. F., Stewart, A. L., Spence, P., and Heywood, K. J.: The Antarctic Slope Current in a Changing Climate, *Rev. Geophys.*, 56,  
741–770, <https://doi.org/https://doi.org/10.1029/2018RG000624>, 2018.
- Tsujino, H., Urakawa, S., Nakano, H., Small, R. J., Kim, W. M., Yeager, S. G., Danabasoglu, G., Suzuki, T., Bamber, J. L., Bentsen, M.,  
et al.: JRA-55 based surface dataset for driving ocean–sea-ice models (JRA55-do), *Ocean Modell.*, 130, 79–139, 2018.
- van Wessem, J. M., van De Berg, W. J., Noël, B. P. Y., van Meijgaard, E., Amory, C., Birnbaum, G., Jakobs, C. L., Krüger, K., Lenaerts, J.,  
525 Lhermitte, S., Ligtenberg, S. R. M., Medley, B., Reijmer, C. H., van Tricht, K., Trusel, L. D., van Uft, L. H., Wouters, B., Wuite, J., and  
van den Broeke, M. R.: Modelling the climate and surface mass balance of polar ice sheets using racmo2: Part 2: Antarctica (1979–2016),  
*Cryosphere*, 12, 1479–1498, 2018.
- Weertman, J.: Stability of the junction of an ice sheet and an ice shelf, *J. Glaciol.*, 13, 3–11, 1974.